Predicting Failure in Multi-bolt Composite Joints using Finite Element Analysis and Bearing-bypass Diagrams

C.T. McCarthy[1, a], M.A. McCarthy[2,b,*] , M.D. Gilchrist[1,c]

[1]Dept. of Mechanical Engineering, University College Dublin, Ireland.

[2]Dept. of Mechanical and Aeronautical Engineering, University of Limerick, Ireland.

[a]conor.t.mccarthy@ucd.ie, [b]michael.mccarthy@ul.ie, [c]michael.gilchrist@ucd.ie

*corresponding author

Keywords: Composites, Bolted Joints, Damage, Finite Element Analysis, Bearing By-pass diagrams

Abstract. A three-dimensional finite element model of a three-bolt, single-lap composite joint is constructed using the non-linear finite element code MSC.Marc. The model is validated against an experiment where the load distribution in the joint is measured using instrumented bolts. Two different joint configurations are examined, one with neat-fit clearances at each bolt-hole and another with a 240 μm clearance at one hole with neat-fits at the others. Bearing and by-pass stresses are extracted from the model and used in conjunction with published bearing/by-pass diagrams to predict the failure load, mode and location for the joints. It is shown that the proposed model accurately predicts the failure behaviour of the joints, as determined from experiments on three-bolt joints loaded to failure. It is also shown that introducing a clearance into one hole significantly changes the failure sequence, but does not affect the ultimate failure load, mode or location. The proposed method demonstrates a simple approach to predicting damage in complex multi-bolt composite joints.

Introduction

Mechanical fastening remains a critical aspect of designing aircraft structures from composite materials, and methods for analysing this problem are constantly improving [1]. Predicting damage and failure in composite joints is a complex task, requiring knowledge of load distribution in the joint and an understanding of the different failure modes associated with different loading configurations. For example, where the ratio of bearing stress to bypass stress at a hole is high the resulting failure tends to be in bearing, and when the ratio is low the failure tends to be in net-tension [2]. To date, most strength prediction studies of multi–bolt composite joints have been based on two-dimensional analytical or finite element approaches [3 -5]. Such two-dimensional approaches cannot be used to study single-lap joints where significant stress concentrations occur in the thickness direction due to bolt bending/rotation and secondary bending in the laminates.

The approach generally taken when predicting failure is to identify the most highly loaded hole [4,6] and to carry out a local failure analysis at that hole using semi-empirical failure criteria, such as that due to Whitney and Nuismer [7]. A drawback with this approach is that a local failure measure does not provide any information on load redistribution (due, for example, to bearing failure at one hole), or the state of sub-critical damage at other holes, before ultimate joint failure occurs.

The aim of this paper is to develop a multi-bolt model that can account for out-of-plane stresses and predict the damage state at each hole in the laminates as the joint is loaded. To do this, a three-dimensional model is constructed using the non-linear finite element code MSC.Marc. This is then used in conjunction with bearing/by-pass stress diagrams to examine the failure mode, location and

load for the joint. To introduce some variation in load distribution, joints with different bolt-hole clearances are examined.

Problem Description

The models are based on experiments carried out on multi-bolt, single-lap composite joints [8]. The joint geometry consists of three bolts "in-line", six washers, three nuts and two composite plates, as shown in Fig. 1. Protruding-head bolts were used and were torqued to a low value (0.5 Nm) to represent a finger-tightened condition. This represents the worst-case design scenario of bolts loosened after fatigue loading and also simplifies the analysis since essentially all the load is taken by the bolts with none taken by friction between the plates. Hence, friction is not considered in this analysis. Washers were used on both the nut and head side. The laminates were made from a carbon fibre/epoxy matrix system (HTA/6376), and were stacked in a quasi-isotropic configuration $[45/0/-45/90]_s$. Both plates were manufactured from 40 plies giving a nominal thickness of 5.2 mm. After assembly, the joint was subjected to a tensile load, applied quasi-statically. In some tests, the joints were loaded in the elastic range and the bolt load distribution was measured using instrumented bolts. In the remaining tests, the joints were loaded until catastrophic failure occurred.

In this paper, results from two joints with different bolt-hole clearance configurations are presented, as shown in Table 1. Joint A represented a control case having a neat-fit clearance at each hole. Joint B had a 240 μm clearance at hole 1, while the other holes had a neat-fit. This was chosen in order to examine the effect of changing the load distribution by introducing a delay in load take-up due to clearance. The bolts were initially centred in the holes in both the experiments and the simulations.

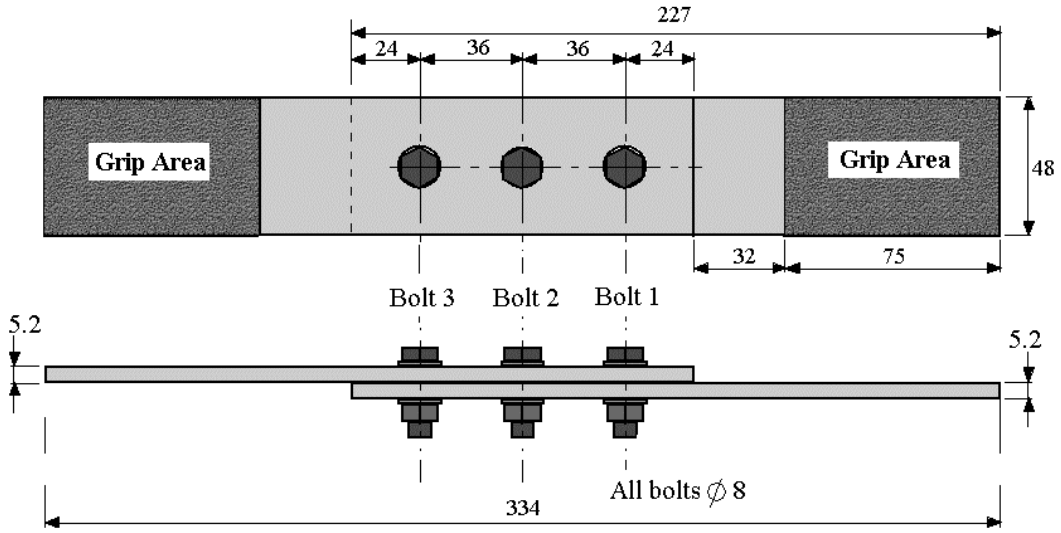

Figure 1 Single-lap, multi-bolt specimen geometry (all dimensions in mm)

Table 1 Bolt-hole clearance cases for the multi-bolt experiments and models

	Bolt/Hole No. 1 Nominal Clearance (μm)	Bolt/Hole No. 2 Nominal Clearance (μm)	Bolt/Hole No. 3 Nominal Clearance (μm)
Joint A	0	0	0
Joint B	240	0	0

Finite Element Model

The finite element model is shown in Fig. 2. Each joint component (i.e. the laminates, washers and bolt) was meshed independently using fully integrated eight-node isoparametric brick elements. For the laminates, a relatively high mesh density was used in the vicinity of the holes where high strain gradients exist.

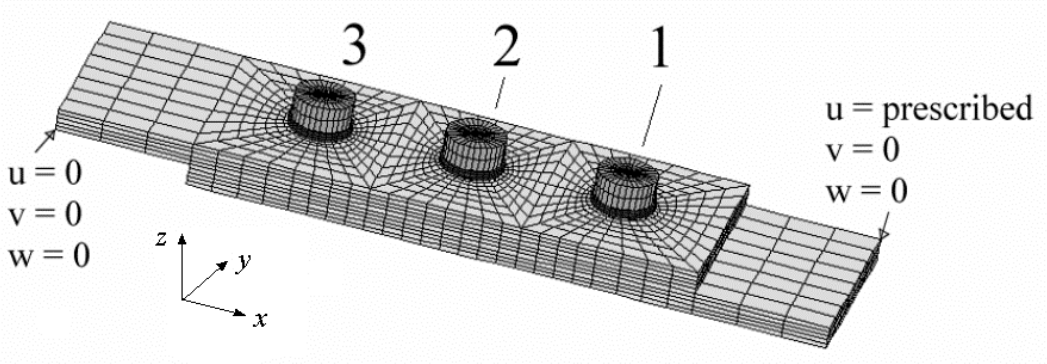

Figure 2 FE model with boundary conditions

The joint model was loaded by applying a fixed boundary condition to all the nodes at the left end of the top laminate, and a prescribed displacement in the *x*-direction to the rightmost end of the bottom laminate with displacements in *y* and *z* fixed, as shown in Fig. 2. To avoid rigid body modes, light springs were attached to components that were not fully constrained, i.e. the laminate with the prescribed end displacement, the bolts and the washers. To simulate bolt pre-load due to the applied bolt torque, orthotropic thermal expansion coefficients (allowing thermal expansion/contraction only in the direction of the longitudinal axis of the bolt) were applied to the washers on one side of the joint. These washers were then subjected to a positive temperature differential prior to mechanical loading which caused the washers to expand which has the effect of stretching the bolts and clamping the laminates, which is essentially what happens experimentally. For the finger-tight torqued experiments modelled here, a bolt pre-stress of 7.2 MPa was applied. This value was obtained experimentally from the axial gauges in the shank of a specially manufactured instrumented bolt [9].

The composite laminates were modelled using a linear elastic anisotropic material and the material properties for HTA/6376 (i.e., the material used in the tests) were obtained from [10]. To avoid modelling each ply of the laminates discretely, homogeneous orthotropic material properties were derived using a homogenisation procedure outlined in [11] and are shown in Table 2. The titanium bolts and steel washers were modelled with isotropic linear elastic material properties, with $E_b = 110$ GPa, $\nu_b = 0.29$ for the bolts, and $E_w = 210$ GPa, $\nu_w = 0.3$ for the washers.

Table 2 Equivalent homogeneous material properties used for the laminates [11]

	E_{xx} (GPa)	E_{yy} (GPa)	E_{zz} (GPa)	G_{xy} (GPa)	G_{xz} (GPa)	G_{yz} (GPa)	ν_{xy}	ν_{xz}	ν_{yz}
Derived Homogeneous Properties from [11]	54.25	54.25	12.59	20.72	4.55	4.55	0.309	0.332	0.332

Contact was modelled using the "direct constraint" method in MSC.Marc. This algorithm requires the definition of "contact bodies", i.e., bodies that potentially may come in contact with each other. To reduce computational effort, only elements on the surfaces of the laminates, washers and bolts

were defined in these contact bodies. An analytical contact description was used to generate a continuous normal over each contact surface of each body. This procedure results in a more accurate representation of the physical geometry [11].

Model Validation

The model was validated by comparing the experimentally measured and predicted load distributions for Joint A configuration (i.e., neat-fit clearances at each bolt-hole). In the experiment, instrumented bolts were used to measure the shear load acting on each bolt and the results are shown in Fig. 3(a). In the model, the bolt loads were determined by summing all x-components of the contact forces acting at each bolt-hole. The resulting load distribution from the model is shown in Fig. 3(b) and, as can be seen, good agreement with the experiment is obtained. Hence, the model was considered sufficiently accurate to proceed with predicting joint strength using bearing/by-pass diagrams.

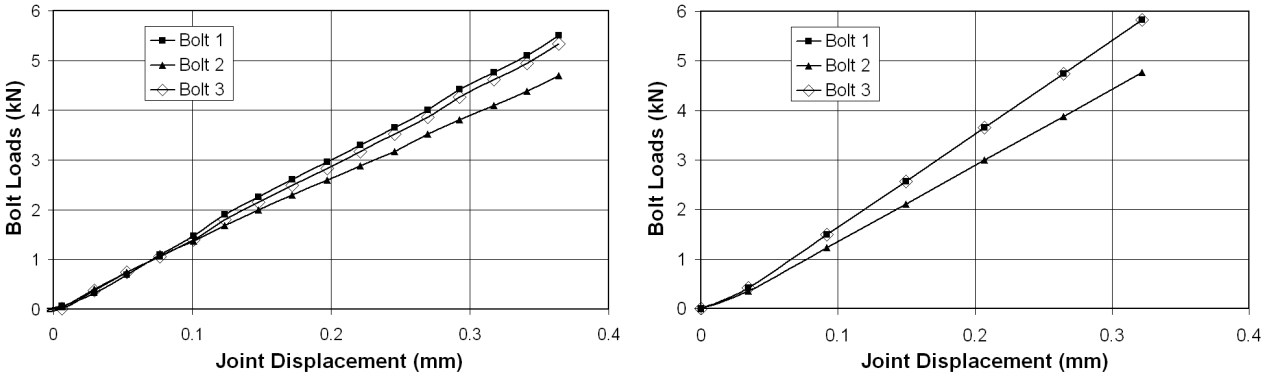

(a) Experiment **(b) Simulation**

Figure 3 Load distribution in Joint A (neat-fit clearances at each hole)

Bearing/By-pass Diagrams

Complex multi-bolt joints can be analysed at a coupon level by assuming that one fastener can be represented by a single-pin joint subjected to both bearing and by-pass loads [12,13]. This assumption has enabled researchers to develop failure envelopes in bearing stress - by-pass stress space which can then be used to predict failure initiation and ultimate failure load, mode and location in composite bolted joints. These diagrams are used here in conjunction with the finite element models to predict the failure load, mode and locations for the multi-bolt joints.

In this paper, only joints subjected to tensile loading are considered. Thus, each hole is in a state of tension-reacted bearing, as shown for a general case in Fig. 4. This figure was taken from Crews and Naik [12], who only considered one hole in a composite specimen which was subjected to both bearing (P_b) and by-pass (P_{bp}) loads. The bearing and by-pass loads were balanced by the "reaction" load, P_a, i.e.,

$$P_a = P_b + P_{bp} \tag{1}$$

To determine the by-pass load at each hole in the three-bolt, single-lap joints, the reaction load, P_a, must be determined at every hole. For example, Fig. 5 shows the loads acting on the top-laminate with hole 2 isolated for analysis. The by-pass load at hole 2 in the top laminate ($P_{bp_{(H2T)}}$) can be determined by rearranging Eq. 1 as:

$$P_{bp_{(H2T)}} = P_{a_{(H2T)}} - P_2 \tag{2}$$

where; P_2 is the bolt load at hole 2 and $P_{a_{(H2T)}}$ is the reaction load at hole 2 and can be determined by considering equilibrium of all the forces to the left of the section, i.e.,

$$P_{a_{(H2T)}} = P_t - P_3 \tag{3}$$

where; P_t is the total applied load and P_3 is the bolt load at hole 3. Hence, the by-pass load can be determined by substituting Eq. 3 into Eq. 2:

$$P_{bp_{(H2T)}} = P_t - P_3 - P_2 \tag{4}$$

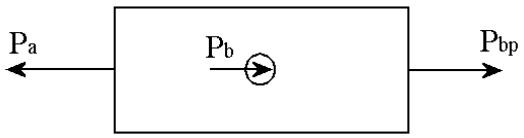

Figure 4 Bearing (P_b), by-pass (P_{bp}) and reaction loads (P_a) in single-hole coupon specimen

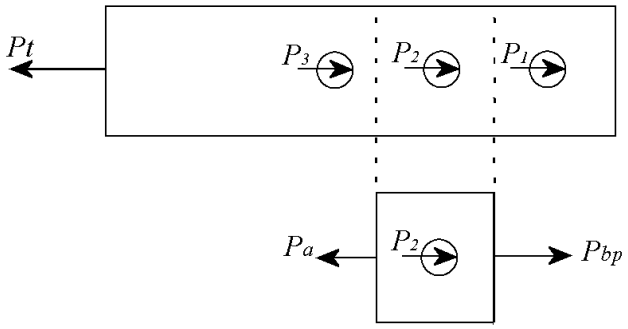

Figure 5 Determining the by-pass (P_{bp}) load at hole 2 in the top-laminate

Following a similar analysis, the by-pass loads for the remaining holes in the top laminate are;

$$P_{bp_{(H3T)}} = P_t - P_3 \tag{5}$$

$$P_{bp_{(H1T)}} = P_t - P_1 - P_2 - P_3 \tag{6}$$

In the absence of friction, the forces acting on the laminates are the total applied load, P_t, and three bolt loads, P_1, P_2 and P_3. For static equilibrium in the loading direction:

$$P_t = P_1 + P_2 + P_3 \tag{7}$$

Hence, the by-pass load at hole 1 in the top laminate (i.e., Eq. 6) is zero. By interchanging the subscripts 1 and 3, the above equations apply to the bottom laminate also.

Before proceeding with the strength analysis, the bolt and by-pass loads must be transformed into bearing and by-pass stresses. The bearing stress at hole i, σ_{br_i}, is determined from the bolt load by the following equation:

$$\sigma_{br_i} = \frac{P_i}{Dt} \tag{8}$$

where: P_i is the bolt load at hole i, D is the hole diameter (note: when a clearance was present, D was taken as the bolt diameter) and t is the laminate thickness. The by-pass stress at hole i, $\sigma_{bp\,i}$, is determined by the following equation:

$$\sigma_{bp\,i} = \frac{P_{bp_i}}{t(W - D)} \tag{9}$$

where: P_{bp_i} is the by-pass load at hole i (given by equations 4 - 6) and W is the laminate width.

Unfortunately, no bearing/by-pass failure envelopes were available for the material used in this study (HTA/6376). Developing such a failure envelope requires a significant amount of testing and a testing machine with two loading actuators, to independently vary the bearing load and by-pass load simultaneously. Development of such a machine was outside the scope of this paper. Instead, the bearing/by-pass failure envelope given by Crews and Naik [12] was adopted here. This failure envelope was generated for a glass/epoxy quasi-isotropic laminate with a 6.35 mm diameter pin. Use of this diagram is justified by the fact that the bearing failure initiation stress and ultimate bearing stress (i.e., the all-bearing case) were determined for HTA/6376 as 520 MPa and 750 MPa respectively [14] and the open hole tensile strength (i.e. all by-pass stress case) was determined as 300 MPa [15] which are all in good agreement with the diagram of Crews and Naik.

Results and Discussion

Joint A: Three tests to failure on this joint configuration were carried out in [16]. The study found that one joint failed in net-tension at hole 1 in the lower laminate at a joint load of 80 kN while another failed by net-tension at hole 3 in the top laminate at 84 kN. The third joint tested failed by bolt failure at 76 kN. It should be noted that bearing damage was evident at holes where bolt failure occurred. However, as this damage mode is non-catastrophic, high loads are transferred through the bolt until high joint loads, causing bolt failure.

The predicted bearing/by-pass diagram is shown in Fig. 6. A star is placed where the bearing/by-pass stress curve intersects the ultimate failure envelope and indicates the failure mode and stress level at which the joint fails. The failure load is determined by evaluating the joint load (i.e. P_t) at which the bearing/by-pass stress curve intersects the failure envelope and this is achieved using equations 4 -9. As can be seen, bearing failures are predicted to initiate (inner envelope) at hole 3 in the bottom laminate and hole 1 in the top-laminate simultaneously which occurred at a joint load of 62 kN. Ultimate failure is subsequently predicted to occur by net-tension at hole 1 in the bottom laminate or hole 3 in the top-laminate, which is in agreement with the experiments This occurred at 67.4 kN, which underestimates the average experimental value by 17.8%.

Joint B: Three tests to failure on this joint configuration were also carried out in [16]. Similarly to Joint A, one joint failed in net-tension at hole 1 in the bottom-laminate at 78 kN and another failed in net-tension at hole 3 in the top-laminate at 82 kN. The third joint tested failed by bolts 2 and 3 failing simultaneously at a joint load of 79 kN.

The predicted bearing/by-pass diagram is shown in Fig. 7. As can be seen, a bearing failure initiates at hole 3 in the bottom laminate and this occurred at a joint load of 56 kN, which is approximately 10% lower than in Joint A. In addition, failure is also predicted to initiate in bearing at hole 2 in the top and bottom laminate at a higher load of 62 kN. Ultimate failure was predicted to occur by a net-tension failure at hole 3 in the top-laminate at a joint load of 67.2 kN. However, it is interesting to note that at a slightly higher load level (68 kN) the hole 1 bottom-laminate bearing/by-pass stress curve intersected the failure envelope at a different location. Hence, although the by-pass stress is considerably higher at hole 1 in the bottom-laminate than at hole 3 in the top-laminate, the combination of bearing and by-pass stresses at these holes result in essentially equal probabilities of failure, which explains the experimental observation. In summary, the failure sequence for this joint is bearing failure initiation at hole 3 in the bottom laminate at 56 kN, followed by bearing failure initiation at hole 2 in the top and bottom laminates at 62 kN and finally, net-tension failure at hole 3 in the top-laminate (or possibly hole 1 in the bottom-laminate) at 67.2 kN. The predicted ultimate failure load is an underestimation of 16% compared to the experimental result but the location of failure and failure mode are in good agreement.

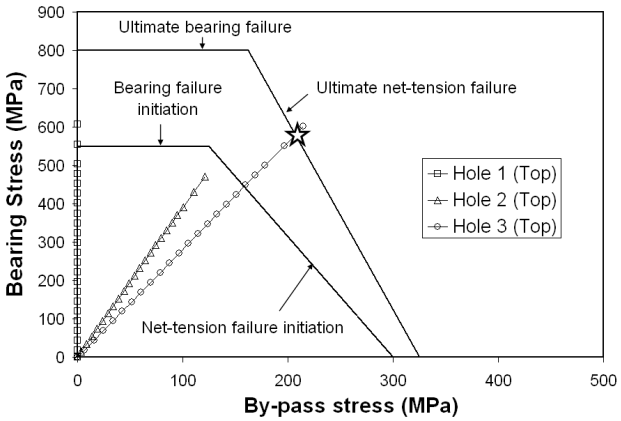

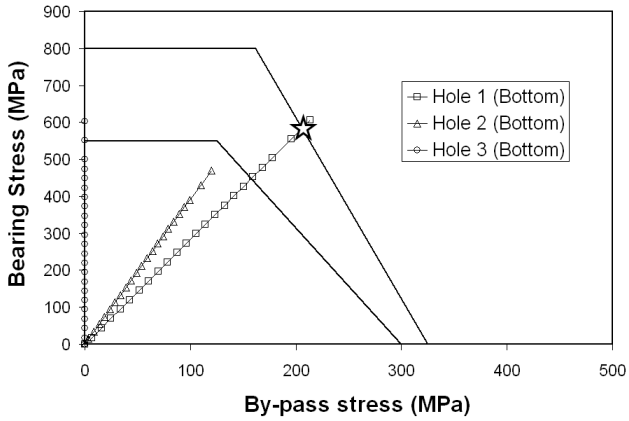

(a) Top-laminate **(b) Bottom-laminate**

Figure 6 Bearing by-pass diagram for Joint A

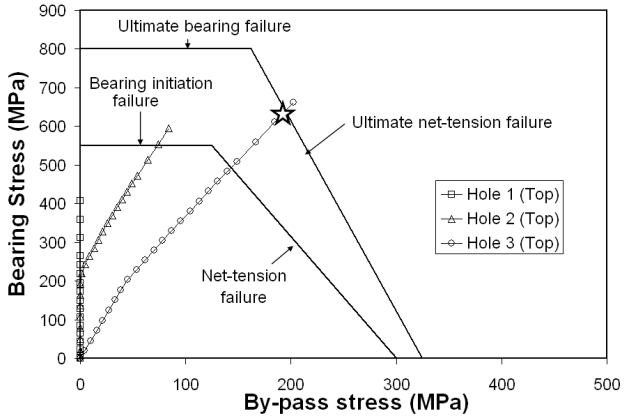

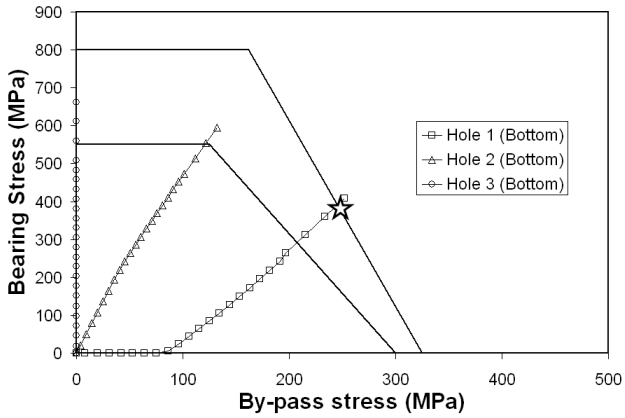

(a) Top-laminate **(b) Bottom-laminate**

Figure 7 Bearing/by-pass diagram for Joint B

Summary: A summary of the experimental and finite element results for failure load, mode and location is given in Table 3. As can be seen, the model predicted the correct failure mode and location with respect to the experimental results but under predicted the failure load by approximately 18%. This was most likely due to using failure envelopes for glass/epoxy and not carbon/epoxy.

Conclusion

In the joint configurations considered, bearing failures initiated before final joint failure. Bolt-hole clearance was found to have a strong effect on the load at which this occurred with bearing failure detected 6 kN earlier in Joint B which had a 240 μm clearance at one hole. However, it was found that clearance did not have a significant effect on the ultimate failure load, mode and location of the joints analysed as both joint configurations were detected to fail by net-tension at either hole 1 in the bottom laminate or hole 3 in the top laminate at approximately 67 kN. Both the failure mode and failure locations were in good agreement with experiments but the predicted failure loads were conservative by approximately 18%, which is due to using a failure envelope for a different material to that used in this study. A drawback with the bearing by-pass diagrams is that they cannot predict bolt failure, which occurred in one case for each of the two joint configurations.

The bearing/by-pass stress curves for each hole in each laminate were plotted in the same diagram which provided a useful graphical method for analysing the behaviour of the joint and provided a clear indication to what was happening with respect to failure at each hole. These diagrams could be

generated automatically as a post processing function and have the potential to provide a useful design tool. It would be possible to generate the bearing/by-pass stress curves in real time (as the simulation is running) in order to reduce analysis time. Once a particular curve intersected the failure envelope (i.e. joint failure detected), the simulation could be stopped. These diagrams could also be used in optimisation studies to help the designer assess the effect of changing a particular variable, such as a bolt diameter or position, for example.

Table 3 Comparison between experiment and simulation for ultimate failure load, failure mode and failure location

Joint	Test No.	Experiment			Simulation		
		Failure Load kN	Failure Mode	Failure Location	Failure Load kN	Failure Mode	Failure Location
A	1	76	BF	H1	67.4	NT	H3 - TL or H1 - BL
	2	80	NT	H1 - BL			
	3	84	NT	H3 - TL			
B	1	79	BF	H2&H3	67.2	NT	H3 - TL or H1 - BL
	2	78	NT	H1 - BL			
	3	82	NT	H3 - TL			

BF – Bolt failure, NT – net-tension failure, H – hole No., TL – top-lap, BL – bottom-lap

References

1. M.A. McCarthy: *Air and Space Europe.* Vol. 3/4 (2001), pp. 139-42.
2. R. Starikov, J. Schon: *Composite Structures.* Vol. 51 (2001), pp. 411-25.
3. S. Wang , Y. Han: *J. Compos Mater.* Vol. 22 (1988), pp. 124-35.
4. B. Sergeev, E. Madenci, D.R. Ambur: *Computers and Structures.* Vol. 76 (2000), pp. 89-103.
5. Y. Xiong: *Int. J. Solid Structures* Vol. 33 (1996), pp. 4395-409.
6. Y. Xiong, O.K. Bedair: American Institute of Aeronautics and Astronautics 1998; AIAA-98-2062.
7. J.M. Whitney, R.J. Nuismer: *J. Compos Mater*. Vol. 8 (1974), pp. 235-65.
8. W.F. Stanley, M.A. McCarthy, V.P Lawlor: *Plastics, Rubber and Composites* Vol. 31 (2002), pp. 412-18.
9. V.P. Lawlor: Ph.D. thesis, University of Limerick, Ireland. 2004.
10. T. Ireman: *Composite Structures Vol* 43 (1998), pp. 195-216.
11. M.A. McCarthy, C.T. McCarthy, V.P. Lawlor, W.F. Stanley: C*omposite Structures 2004*. In-Press.
12. J.H. Jr. Crews, R.A. Naik. National Aeronautics and Space Administration 1987; NASA TM 89153.
13. L.J. Hart-Smith, 1976. NASA Contractor Report, NASA CR-1444899.
14. D. Hachenberg, 2001, Personal Commuication. Airbus Deutschland.
15. Ball, P., 2003. Personal Commuication, Airbus UK.
16. McCarthy, M.A., V.P. Lawlor, W.F. Stanley, 2004, *J. Compos Mater. (2004),* In-press.